Fluorine Plasma Treatments of Polypropylene Films, 1 – Surface Characterization[a]

Seth Kirk,* Mark Strobel, Chi-Ying Lee, Steven J. Pachuta, Michael Prokosch, Hyacinth Lechuga, Marvin E. Jones, Christopher S. Lyons, Scott Degner, Yang Yang, Mark J. Kushner

In this work, an experimental investigation of fluorine gas (F_2) plasma treatment of polypropylene (PP) film reveals the evolution of PP fluorination. Surface analysis of fluorinated PP surfaces describes a surface modification process that is initially quite rapid but slows sharply as the fluorination progresses. The fluorination reaction occurs more rapidly at the PP film surface and evidence of a treatment gradient is seen in the ESCA sampling depth of 10 nm. The increasingly fluorinated surface becomes less reactive to the plasma chemistry and develops a fully fluorinated, cross-linked surface layer that eventually extends the full ESCA sampling depth.

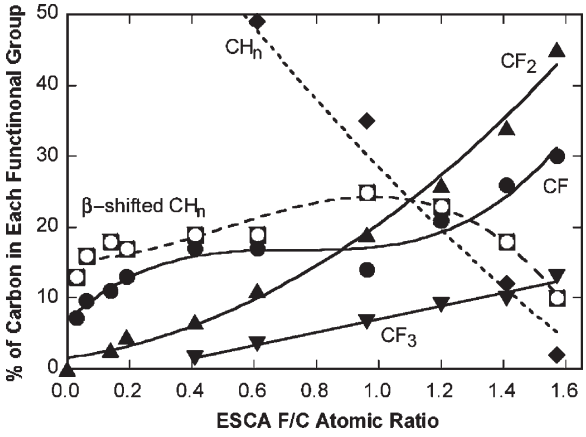

Introduction

Surface fluorination has long been investigated as a method of economically providing the valuable surface properties of fluorocarbon polymers on low-cost commodity polyolefin materials.[1] Commercially desirable surface properties of fluoropolymers include hydrophobicity, oleophobicity, and release (non-adhesion).

S. Kirk, M. Strobel, C.-Y. Lee, S. J. Pachuta, M. Prokosch, H. Lechuga, M. E. Jones, C. S. Lyons, S. Degner
3M Company, 3M Center, Building 208-1-01, St. Paul, MN 55144, USA
Fax: (+651) 733 3304; E-mail: smkirk@mmm.com
Y. Yang
Department of Electrical and Computer Engineering, Iowa State University, Ames, IA 50011, USA
M. J. Kushner
Department of Electrical Engineering and Computer Science, University of Michigan, 1301 Beal Avenue, Ann Arbor, MI 48109, USA

[a] Part 2: cf. ref.[11]

There are several viable industrial approaches to fluorinating the surfaces of polyolefins such as polyethylene (PE) and polypropylene (PP). The process of direct fluorination is performed by direct exposure of polymer surfaces to dilute mixtures of F_2 in inert gases such as nitrogen or argon at atmospheric pressure.[2] Plasma fluorination uses fluorine-containing gases introduced to a low-temperature plasma to create polymer surface fluorination. This process can be used with non-polymerizing gases, including some fluorocarbons, such as CF_4 or C_2F_6, or inorganic fluorides, such as SF_6.[3] The plasma polymerization of fluorocarbons, such as C_2F_4 or n-C_4F_{10}, is another method that has been used to generate fluorinated surfaces on polyolefins.[4] The only reported experimental investigations of F_2 plasmas for polymer surface modification were performed by the group of Cohen and Baddour in the late 1970s and early 1980s.[5–10]

In this paper, we report on investigations of F_2/Ar plasmas as a method for fluorinating PP films in an industrially viable, continuous treatment process. The treatment of a hydrocarbon polymer surface using an F_2-containing plasma results in an experimental system

© 2010 WILEY-VCH Verlag GmbH & Co. KGaA, Weinheim
DOI: 10.1002/ppap.200900111

with exceptional clarity. The relatively simple reactive chemistry of F_2/Ar plasma, combined with surface analysis techniques that are capable of distinguishing fine differences in fluorinated polymer surfaces, allows for detailed characterization of the polymer surface fluorination reaction. Our investigations utilized a mechanical system for the transport of polymer film through a plasma, which allowed us to investigate short residence times and accordingly allowed us to examine the full development of the fluorination reaction on the polymer film.

In Part 2 of this paper,[11] we report the results from an integrated plasma and surface kinetics model that was developed simultaneous with the reported experimental work to describe the reactions in the F_2/Ar plasma treatment of a PP film surface.

Experimental Part

Biaxially oriented isotactic PP film was the substrate used in this study. The 0.05-mm-thick PP film was produced using a homopolymer resin with a weight-average molecular weight of 3.6×10^5, a polydispersity index of 4.0, and a peak melting temperature of 163 °C. The base resin contained ca. 200 ppm of an inorganic acid scavenger and ca. 1 000 ppm of high-molecular-weight phenolic antioxidants. The additives are not detectable by X-ray photoelectron spectroscopy (XPS or ESCA) and are detected only at very low levels by time-of-flight static secondary ion mass spectrometry (ToF-SIMS).

The plasma treatments were performed using a reactor built by 3M Company, configured as shown schematically in Figure 1 and connected to a vacuum pump stack consisting of a Roots blower and a mechanical "dry" pump. The aluminum treatment chamber contained large-area flat-plate aluminum electrodes spaced 2.54 cm apart and a simple speed-controlled system for transporting a polymer film from a source roll, through the center of the space between the electrodes, to a collection roll. Film transport speeds between 3.5 and 51 $cm \cdot s^{-1}$ were used and the total path length for the film between the electrodes was 91 cm, providing a residence time of 1.8–26 s. Compressed F_2 gas (Air Products, >97% purity) and argon (Oxygen Service Co., industrial grade, <5 ppm O_2, <10 ppm H_2O) were metered through mass flow control systems (Brooks Instrument model 5850EM). The fluorine and argon flows were combined in a gas manifold and then introduced as a mixture through an array of 1.6-mm-diameter exit holes located across the face of the electrode. Because the experimental system had a maximum transport speed, it was necessary to use different concentrations of fluorine gas, in addition to varying polymer film speeds, to create samples with reduced degrees of fluorination at achievable exposure times. The reported samples were created using a feed gas that contained 0.7% F_2, 10% F_2, or 60% F_2 in argon. The electrodes were connected to a 13.56 MHz power supply (RF Power Products, Inc., Model RF50SWC) through a matching network (RF Power Products, Inc., Model 7621020020). The power supply was operated at a level that provided 0.18 $W \cdot cm^{-2}$ of electrode area or 0.07 $W \cdot cm^{-3}$ of plasma volume. The power supply had an optional pulsing control that, when activated (during experiments

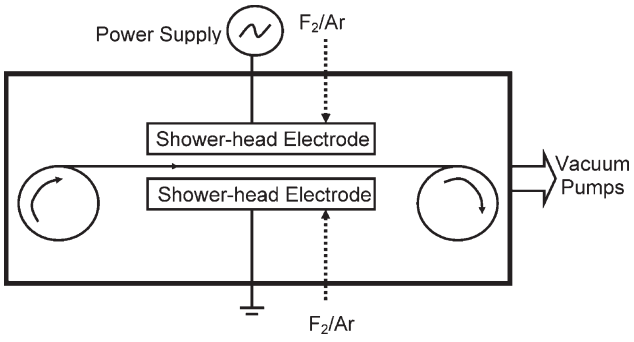

Figure 1. Schematic diagram of the plasma fluorination reactor.

that used an F_2 concentration of 10% or less), produced a 10 ms "on" pulse every 100 ms.

Our experimental system differs from the system used by Cohen and Baddour.[5–10] They used a radio-frequency (13.56 MHz) inductively coupled plasma sustained in mixtures of either 5 or 15% F_2 in helium or argon. Their small quartz reactor with an internal volume of ca. 8 L that was typically held at pressures of 2–3 Torr. Plasma powers were typically 3–12 $W \cdot cm^{-3}$ of plasma volume. Exposure times from 15 s to several minutes were studied. While most of the work of Cohen and Baddour was performed using low-density PE film as the substrate, some data[8] were reported for the fluorination of PP, poly(vinyl fluoride), polystyrene, and other polymer films. They did not report the use of higher concentrations of F_2 in the plasma, capacitively coupled discharges, or short-exposure, low-power treatments.

For our experimentation, the reactor was typically evacuated to a base pressure of approximately 20 mTorr. After evacuation, the F_2/argon gas mixture was introduced to the chamber at total flow rate of 8 $L \cdot min^{-1}$, which produced a steady pressure of approximately 500 mTorr during each experiment. When evacuated to base pressure and sealed, the rise in system pressure indicated a 12 standard $cm^3 \cdot min^{-1}$ leak rate. This leak rate indicates that during the plasma treatments there was a 0.15% concentration of air (or a 300 ppm O_2 concentration) in the process gas.

At the start of each plasma treatment experiment, a 1-min equilibration period was used before the film translation was initiated. Approximately 15 m of polymer film was treated at each condition before a representative sample was collected.

Polymer films treated in the F_2 plasma process were analyzed by ESCA, contact angle measurement, ToF-SIMS, and atomic force microscopy (AFM). ESCA data were acquired using a Kratos AXIS Ultra DLD spectrometer (Kratos Analytical Ltd., Manchester, UK) with a monochromated Al Kα X-ray source. All reported compositional measurements were acquired at a photoelectron take-off angle of 90° in the "hybrid mode" (take-off angle is defined as the angle between the sample surface and the axis of the ESCA analyzer lens). A low-energy electron flood gun was used to minimize surface charging. The typical X-ray spot size was 700 $\mu m \times 300$ μm. For each sample, an initial compositional survey scan was acquired using a pass energy of 160 eV. High-resolution C 1s spectra were acquired using a pass energy of 20 eV and were charge-referenced to the C 1s hydrocarbon peak set to 285.0 eV. Data analysis was performed with Vision Processing data reduction software (Kratos Analytical Ltd.) and CasaXPS (Casa Software Ltd.). Two or more

© 2010 WILEY-VCH Verlag GmbH & Co. KGaA, Weinheim
DOI: 10.1002/ppap.200900111

areas of each film sample were analyzed and averaged to obtain atomic percent (at.-%) values for each sample. F/C ratios were calculated from the average at.-% determined from the survey spectra. Details of the technique used to estimate the surface structure from the high-resolution C 1s ESCA spectra are described in the Results Section.

Measurements of the advancing and receding contact angles in air of deionized, filtered water and hexadecane ($C_{16}H_{34}$) were made using the Wilhelmy plate method on a ThermoCahn Radian DCA 322 dynamic contact-angle instrument. Using the ThermoCahn microbalance, the surface tensions of the water and the hexadecane were measured as 72.4 and 28.7 $mN \cdot m^{-1}$, respectively. A three-layer laminate was prepared using 3M Scotch Brand #666 double-coated tape to mount the treated sides of the film outward. To prevent contamination during the preparation of this laminate, the treated surfaces only contacted untreated PP film, a situation analogous to the common practice of winding modified film into roll form after treatment. The laminate was cut into a 2.6 cm × 2.6 cm square for analysis. The stage speed was 50 $\mu m \cdot s^{-1}$ with a sample submersion distance of 6 mm. For both contact-angle probe liquids, the motion of the stage was halted for 1 min at the position of maximum travel prior to starting the retraction phase of the Wilhelmy cycle, thereby soaking the sample in the liquid for a period of time. The volume of liquid used for the contact-angle measurements was ca. 50 cm^3, with a fresh volume used for each sample analyzed. The advancing and receding contact angles were calculated using a software routine supplied with the ThermoCahn instrument that uses linear regression for the buoyancy correction. The untreated PP film had advancing and receding water contact angles of 109° and 87°, respectively, while the hexadecane contact angles on untreated PP were 0°. Each reported contact-angle value is the average of three individual measurements. Typical standard deviations for the contact-angle measurements were 2°. A detailed gauge repeatability-and-reproducibility study of the Wilhelmy method showed that none of the variance in the contact-angle measurements could be attributed to operator-to-operator variability. All of the variability in the contact angles that we measured was "part-to-part" caused by minor variations in the identically treated samples of film.

During the measurement of the reported contact angles, samples were analyzed by a secondary immersion into the test liquid. This additional measurement provided data similar to what would be measured on samples that are washed before the collection of contact angles. For all of the reported results, there were no significant differences between the advancing or receding contact angles measured during the first and second immersions in the test liquids, so only first-immersion results are reported. In addition, this analysis indicated that there was no significant reactivity between the analyzed surfaces and either test liquid.

ToF-SIMS analysis was performed on samples using an ION-TOF, GmbH (Münster, Germany) TOF.SIMS.5 instrument, with a 25 kilovolt (keV) Bi^+ primary ion beam and a pulsed current of approximately 0.5 pA, rastered over a 500 μm × 500 μm sample target area. The extraction potential was fixed at 2.0 keV. Charge neutralization was accomplished using a pulsed electron gun, cycled every primary ion pulse. A detector post-acceleration voltage of 10 kV was employed. Beam bunching was used to reduce the pulse width and improve spectral mass resolution. The mass resolutions at mass 69 in the positive and negative ion spectra were typically >4 000 full-width at half-maximum (FWHM). The spectral cycle time was 150 μs. Using these conditions, the total primary ion dose during a typical 2-min acquisition was below the static limit.[12] ION-TOF IonSpec version 4.1 software was used in the acquisitions, while a custom-written TOF-SIMS data processing package was used for data processing. Measurements were collected from two separate locations on each sample and the results were averaged.

The unmodified and fluorinated PP films were examined using a Digital Instruments Multimode SPM atomic force microscope (AFM) operated in the tapping mode. OTESPA etched-silicon cantilever probes, which have nominal spring constants of ca. 42 $N \cdot m^{-1}$, resonant frequencies of ca. 300 kHz, and estimated radii of curvature of 7.5 nm were used. The typical A_{sp}/A_o setpoint ratio used for imaging was 1.3/1.8, where A_{sp} is the amplitude of the cantilever oscillation (in volts) at the imaging setpoint and A_o is the amplitude of the cantilever oscillation (in volts) in free space. The integral and proportional feedback gains were typically 0.3 and 0.4, respectively. Scan rates were 0.8–1.0 Hz for 2 μm × 2 μm images. To ensure that the information that we obtained from AFM accurately represented the topography of our PP films, numerous examinations were made of each pertinent sample. Characteristic images are shown in this paper. In all of the images shown, the range from the darkest to the lightest tone represents 50 nm of height in the *z*-direction and the area of PP film imaged was 2 μm × 2 μm.

While each of the reported measurement techniques is considered to be a surface-analysis technique, it is important to note that each technique probes different depths of the polymer film "surface." Briggs[13] considers that the ESCA sampling depth for carbon atoms using 90° take-off angle ESCA is approximately 9 nm, although a larger proportion of the ESCA signal originates from atoms closer to the surface. Briggs further describes the sampling depth of ToF-SIMS to be "on the order of 1 nm." Zisman[14] estimates that liquid contact angles are also sensitive to the outermost 1 nm of a solid surface.

AFM analysis maps the surface topography with presumably no penetration into the molecular structure of the polymer. The AFM images included here show roughness with a height variation of 50 nm over a 2 μm × 2 μm section. As previously noted, the reported ToF-SIMS analysis collects data from a 500 μm × 500 μm section, the ESCA analysis collects data from a 700 μm × 300 μm section, and the contact angle data averages the response of a 5.16-cm-long liquid front that traverses 6 mm during the analysis.

Results and Discussion

Experiments

The goal of our experimentation was to produce samples that reveal the progression of the PP surface fluorination reaction. Although we used multiple experimental conditions to produce the reported samples, the combined analytical results produce trends that are continuous with respect to the degree of fluorination of the treated PP. Additionally, none of the reported treatments produced visually observable distortion or color changes to the films.

© 2010 WILEY-VCH Verlag GmbH & Co. KGaA, Weinheim

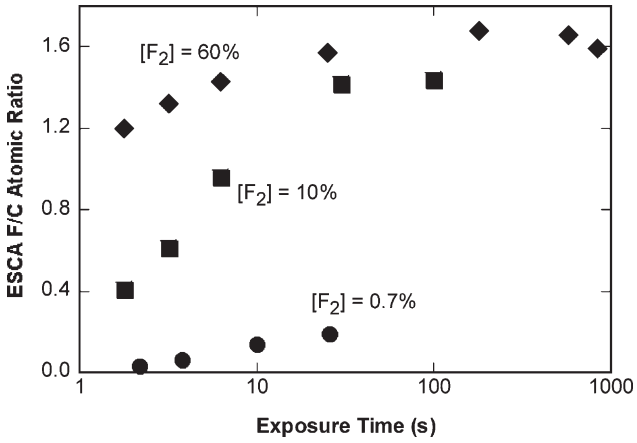

Figure 2. ESCA F/C ratio of fluorinated PP as a function of plasma exposure time for the three experimental conditions.

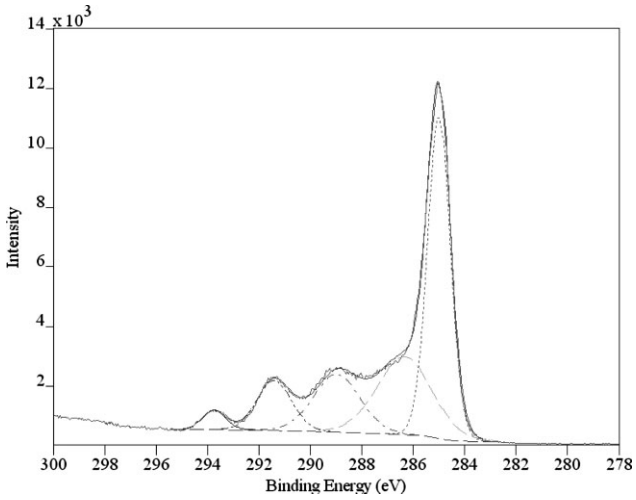

Figure 3. Best fit of high-resolution ESCA C 1s spectrum of PP treated with a 10% F_2/Ar plasma for 3.2 s. The ESCA F/C ratio calculated from survey spectra is 0.61.

ESCA Results

The ESCA F/C atomic ratio of fluorinated PP samples, as a function of exposure time, is shown in Figure 2. These representative samples, selected from a set of dozens of analyzed samples, indicate that initial fluorination, approximately up to an F/C of 1.2, occurs within a few seconds for treatments using a 60% F_2 concentration. These data further indicate that the rate of change of the F/C ratio with exposure time decreases rapidly after an F/C of ca. 1.4 is attained.

Typical ESCA C 1s spectra of a moderately fluorinated (F/C = 0.61) and a highly fluorinated (F/C = 1.57) PP film sample are shown in Figure 3 and 4, respectively. The clearly defined peaks in these representative spectra show that there is minimal ambiguity in the indicated ESCA peak fits.

If the reported fluorination treatments only resulted in the substitution of fluorine atoms for hydrogen in the PP structure, then six types of fluorinated species would be possible: $-CF_3$, $-CF_2-$, $-CHF_2$, $-CHF-$, $-CH_2F$, and $-CF-$, in addition to unfluorinated species, CH_n. A surface containing only these species would result in five distinct peaks in the C 1s spectra. The species $-CF_2-$ and $-CHF_2$ would have the same binding energy in the ESCA spectra, as would the species $-CHF-$, $-CH_2F$, and $-CF-$. The C 1s spectra would show two distinct binding energy levels for the CH_n species; the base signal and a distinct β-shifted signal arising from non-fluorinated carbon atoms that are located immediately adjacent to fluorinated carbon atoms.

ESCA detected minor amounts of oxygen on the surfaces of all of our analyzed samples, except for the untreated polymer. This same result was seen in the work reported by Anand et al.,[7] who note that even small amounts of oxygen in a plasma are highly reactive with polymer surfaces. Anand et al. postulated that the increase in surface oxygen concentration seen on treated polymer films might be caused by post-reaction of sub-surface radicals with atmospheric oxygen. However, Occhiello et al.[15] examined the plasma treatment and post-reaction of a PP surface using isotopic O_2 and demonstrated that the oxidation of the plasma-treated PP occurs by reaction in the plasma and not by exposure of the plasma-treated surface to air after treatment.

For all our treated samples, the surface fluorine concentration was significantly higher than the surface oxygen concentration. The ESCA O/C ratio as a function of the ESCA F/C ratio is shown in Figure 5. These data show that some samples with a relatively low F/C value exhibited relatively high concentrations of oxygen on the surface. We consider the oxygen concentration to be insignificant for

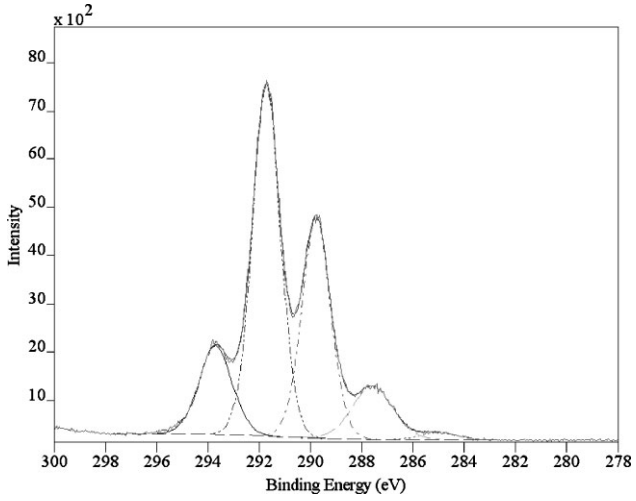

Figure 4. Best fit of high-resolution ESCA C 1s spectrum of PP treated with a 60% F_2/Ar plasma for 25.3 s. The ESCA F/C ratio calculated from survey spectra is 1.57.

© 2010 WILEY-VCH Verlag GmbH & Co. KGaA, Weinheim
DOI: 10.1002/ppap.200900111

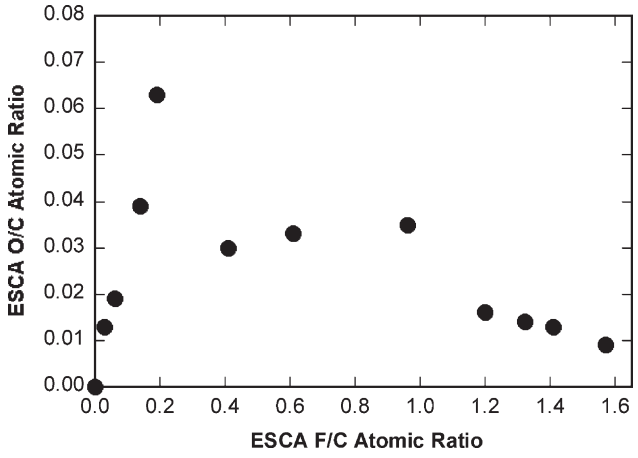

Figure 5. ESCA O/C ratio as a function of ESCA F/C ratio for PP exposed to an F_2/Ar plasma.

those samples having an F/C ratio above 0.5. Above this value, all samples had at.-% O of less than 2.0 and we assume that the character of the ESCA spectra is explained solely by the fluorination state. Below an F/C value of 0.5 the range of at.-% O was between 5.0 and 1.2 and the surface oxygen is included in the ESCA signal ascribed to the CF and β-shifted CH_n species.

The binding energy shifts relative to the assigned 285.0 eV for CH_n for a series of fluorinated films are shown in Figure 6. Note the general progression to higher binding energy shifts as fluorination increases. These results reflect the fact that, as the extent of fluorination increases, these groups are found in environments that are progressively more fluorinated on the average. For example, as the three carbon atoms adjacent to a CH group become increasingly fluorinated, the β-shift effect on that CH group will increase, thereby increasing the binding energy shift.

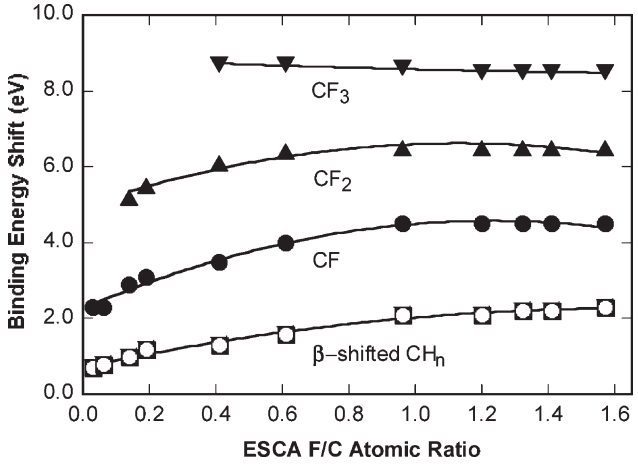

Figure 6. ESCA C 1s component binding energy shifts as a function of F/C ratio for PP exposed to an F_2/Ar plasma. The fitted lines have no significance other than to guide in the viewing of the data.

Because the β-shifted CH_n peaks are strongly differentiated, the non-β-shifted CH_n peaks have binding energies that are largely independent of the chemical environment in which they are found. Carbon atoms in CF_3 groups will also have binding energy shifts independent of the chemical environment in which they are found because they are inherently more fluorinated than any neighboring carbon in the polymer. Our results validate the reference of C 1s ESCA spectra to the 285.0 eV binding energy for hydrocarbon because, even at high F/C ratios, the separation between the non-β-shifted CH_n and the CF_3 groups is the expected amount of approximately 8.8 eV.[16]

Our reported binding energy shifts generally fall within the range reported in the literature. Reported binding energy shifts are: β-shifted CH_n: 0.6–1.8 eV, CF: 2.9–4.8 eV, CF_2: 5.8–6.8 eV, and CF_3: 8.7–10.0 eV.[1,16–19] One exception to the agreement between our experimental results and previously reported binding energy values is the shift of the β-shifted CH_n groups in highly fluorinated samples. By considering the reported effects of fluorine substitution on observed binding energy shifts, it is reasonably estimated that carbon atoms or CH_n groups that are bound only to other highly fluorinated carbon atoms may produce binding energy shifts of greater than 2 eV.

A further exception to the agreement between our analysis shown in Figure 6 and literature values of binding energy shifts is the binding energies estimated for the CF and CF_2 peaks in samples with low F/C ratios. We presume that the relatively low fluorine concentration and the relatively high oxygen concentration on these samples are associated with these atypical values.

In addition to changes in binding energy shifts with increasing extent of fluorination, we also observe trends in the widths of the peaks observed within the C 1s spectra. Peaks that indicate CH_n and CF_3 functionalities in the high-resolution C 1s spectra of reported samples have generally low FWHM values, but because of the many different chemical environments possible for CF or the β-shifted CH_n, peaks from these species can be broad. The ESCA C 1s spectra FWHM for the CF and the β-shifted CH_n peaks are shown in Figure 7. For these peaks, the change in the FWHM with increasing degree of fluorination indicates that chemical heterogeneity first increases, then decreases, as the fluorination of the PP surface continues. As shown, the FWHM for the CF groups reaches a maximum at low F/C values, but the maximum FWHM for the β-shift CH_n peak occurs approximately at the midpoint of fluorination. These FWHM data indicate that the greatest variety of CF species occurs at lower F/C ratios but the greatest variety of β-shifted CH_n species occurs at moderate F/C ratios.

The percentages of total carbon atoms in each functional group, as derived from the ESCA C 1s spectra, are shown in Figure 8. This data set shows general trends of decreasing CH_n species and increasing CF, CF_2, and CF_3 species. The

© 2010 WILEY-VCH Verlag GmbH & Co. KGaA, Weinheim

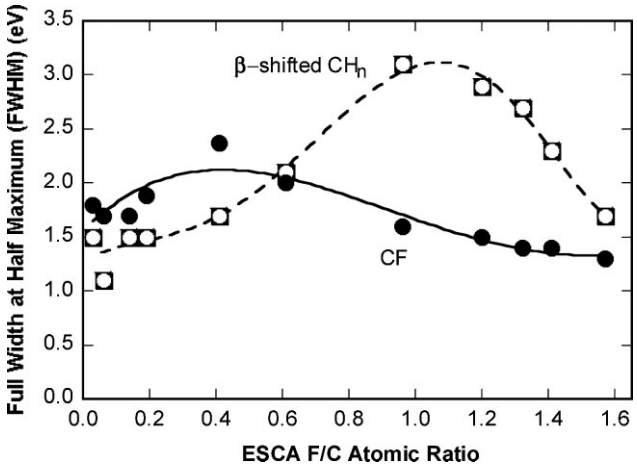

Figure 7. ESCA C 1s CF and CH_n component FWHM measure as a function of F/C ratio for PP exposed to an F_2/Ar plasma. The fitted lines have no significance other than to guide in the viewing of the data.

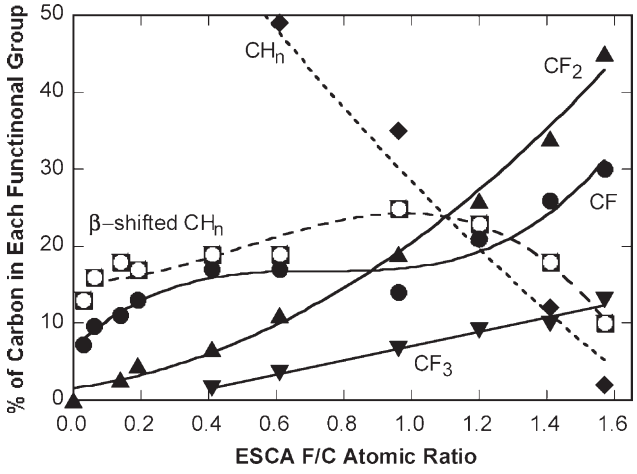

Figure 8. Percent of C atoms in each functional group, as indicated by the best fit of ESCA C 1s spectra, as a function of F/C ratio, for PP exposed to an F_2/Ar plasma. The fitted lines have no significance other than to guide in the viewing of the data.

β-shift CH_n signal rises early in the progression of fluorination, then falls off as the fluorination process ends. The magnitude of the β-shift CH_n signal reaches a maximum near the mid-point of fluorination.

A selection of fluorinated PP films were also analyzed using grazing-angle ESCA analysis with a 15° take-off angle. The comparison of grazing-angle ESCA results to those of normal-angle ESCA results can indicate variation in the structure of the fluorination over the outermost ≈9 nm of the treated sample surface. More electrons are sampled from material closer to the surface and this attenuation of electron ejection is enhanced if electrons are detected at smaller angles to the surface. However, the grazing-angle ESCA indicated F/C ratios that were only slightly higher than the F/C ratios indicated by normal-angle ESCA. The trend of fluorinated group development observed in the grazing-angle ESCA was generally similar to the trend observed in the normal-angle ESCA. The F/C ratios from the grazing-angle analysis had a relatively larger difference from the normal-angle F/C ratios in samples with lower extent of fluorination.

Overall, ESCA indicates that with increasing exposure to a F_2/Ar plasma, a PP surface experiences continually increasing extent of fluorination, although the changes in fluorination occur rapidly at first and more slowly in the latter stages of the reaction. Apart from these general trends, one result of note is that even with extreme exposure times, no sample showed an F/C ratio greater than 1.57. This and other deviations from a general trend of random fluorination of a PP polymer will be discussed below.

AFM Results

The surface topography of the fluorinated PP film samples was examined using AFM. Representative AFM images of treated PP films are shown in Figure 9. The AFM image shown in Figure 9(a) was collected from a fluorinated PP film sample with an F/C ratio of 0.61. AFM images of all treated samples with lower amounts of fluorination appeared similar. Figure 9(a) shows the characteristic fibrillar structure of our PP film and appears similar to previously reported images of an untreated PP surface.[20] This image also shows that no discernable topographical change occurs on fluorinated PP surfaces with F/C ratios of ca. 0.6 or less. An image of a fluorinated PP film with an F/C ratio of 0.93 is shown in Figure 9(b) and indicates the development of fibrils with nodular features. At a higher F/C ratio of 1.32, the nodular character becomes more prominent, as seen in Figure 9(c). At an F/C ratio of 1.57, the fibril structure is completely disrupted and only nodular features remain, as seen in Figure 9(d). Although the topography shown in Figure 9(d) is substantially different from that in Figure 9(a), the root-mean-squared roughness (R_q) increases only slightly between these samples. The mean R_q values calculated for samples imaged in Figure 9(a)–(d) are 5.2, 5.7, 7.8, and 8.0 nm, respectively.

Previous work has reported AFM characterization of PP surfaces oxidized by flame and corona treatment.[20,21] The nodular fibrils in Figure 9(b)–(c) have similarities to structures seen in AFM images of flame-treated PP, but are distinctly different from AFM images of PP oxidized by corona treatment. In work examining PP oxidation, Strobel et al.[20] demonstrated that PP surfaces with the same extent of oxidation created by flame or corona have different degrees of polymer scission. They attributed the

© 2010 WILEY-VCH Verlag GmbH & Co. KGaA, Weinheim
DOI: 10.1002/ppap.200900111

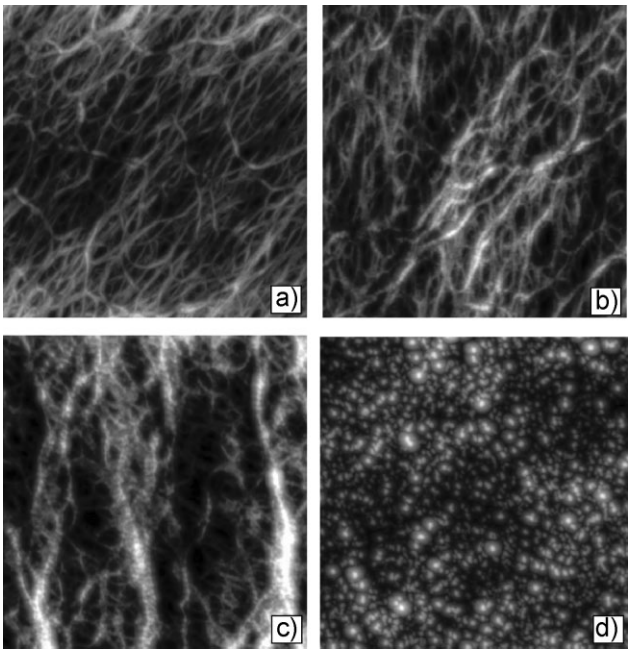

Figure 9. AFM images of PP treated with (a) 10% F_2/Ar plasma for 3.2 s (PP F/C = 0.61), (b) 10% F_2/Ar plasma for 6.3 s (PP F/C = 0.93), (c) 60% F_2/Ar plasma for 3.2 s (PP F/C = 1.32), and (d) 10% F_2/Ar plasma for 25 s (PP F/C = 1.57). Each imaged area of treated PP is 2 μm × 2 μm and the range from the darkest to the lightest tone represents 50 nm of height in the *z*-direction.

nodular topography of flame-treated PP films to the formation of "tethered," higher-molecular-weight scission products, while the larger, soluble structures on the corona-treated surface were characterized as agglomerated lower-molecular-weight polymer scission products.

Although the PP films treated in F_2/Ar plasmas show some degree of oxidation, there is no evidence that the oxidation of the fluorinated PP can be attributed to the observed changes in the AFM images. Jones et al.[21] reported that changes in the AFM images of PP fibrils were observed at an O/C ratio of ca. 0.05 for the flame-treated films and at an O/C ratio of ca. 0.03 for the corona-treated PP films. The highest oxidation level observed in the fluorinated PP samples was 0.06 and occurred in a sample with an F/C ratio of 0.19, where no change in surface topography was evident. Nodular topography on the fluorinated PP films was observed for all samples having an F/C ratio greater than approximately 0.6. As shown in Figure 5, these more-fluorinated samples all have O/C ratios of 0.035 or less, at about the threshold for observable change that was reported by Jones et al. O/C ratios are quite low on the most-fluorinated samples, as shown in Figure 5, indicating that the fluorination process induces a restructuring of the PP surface distinct from oxidation.

The topography change in a PP film due to plasma fluorination has been previously reported by Hopkins and Badyal.[22] Hopkins and Badyal used long exposures of PP to a plasma containing CF_4, a non-polymerizable gas whose predominant reactive component in a plasma environment is fluorine atoms. Hopkins and Badyal showed that the fibrillar structure of the PP film prior to treatment was replaced by large, globular features after CF_4 plasma treatment. These globular features were much larger than the features observed in our samples and were also significantly altered by washing with organic solvents. Hopkins and Badyal proposed that the globular mounds were caused by the formation of low-molecular-weight species as a result of ion bombardment, vacuum ultraviolet irradiation, and chemical attack by fluorine atoms during treatment.

The difference in the AFM analysis of fluorinated PP reported by Hopkins and Badyal[22] and our reported work is similar to the difference between the two oxidative systems reported by Strobel et al.[20] Considering solvent washing and AFM analysis, Strobel et al. noted that the different reaction pathways of PP oxidation by flame or corona result in similar levels of PP oxidation but with differing degrees of polymer scission. As noted previously, the samples reported here had no significant changes in contact angles after washing. Strobel et al. correlated changes in contact angles after washing with the dissolution of low-molecular-weight species. This suggests that, although Hopkins and Badyal achieved similar extent of fluorination compared with the work reported here, the longer exposures used in that work resulted in a different surface structure in the final fluorinated state.

It has also been demonstrated that disruption of the fibrillar structure is not caused by surface melting. Strobel et al.[20] compared treatments of PP film with oxidizing and reducing flames that delivered a similar thermal flux to the PP surface but with different reactive chemistry. In the conditions examined, the oxidizing flame resulted in the development of a nodular topography while the reducing flame did not. We have also characterized the surface of an untreated PP film that was exposed to a gas-fired "IR burner." This was done in a continuous pass at 8 m · min^{-1} for a total exposure time of approximately 0.8 s. This treatment produced a mild distortion of the film, so it is assumed that this treatment delivered a thermal load to the PP film that was relatively close to the amount needed to soften and melt the film. AFM images of this sample appear identical to the AFM images of the untreated film. This suggests that the changes observed by AFM analysis of the highly fluorinated films are not thermally induced.

Contact Angle Results

The advancing and receding contact angles of water and hexadecane (shown in Figure 10 and 11) were measured on

© 2010 WILEY-VCH Verlag GmbH & Co. KGaA, Weinheim

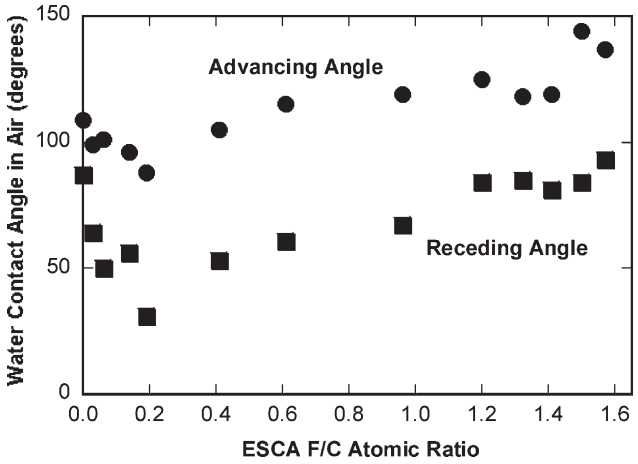

Figure 10. Water contact angles as a function of ESCA F/C ratio for PP exposed to an F_2/Ar plasma.

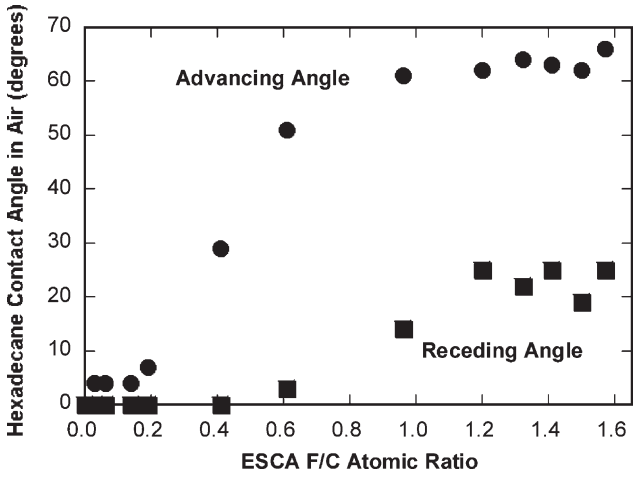

Figure 11. Hexadecane contact angles as a function of ESCA F/C ratio for PP exposed to an F_2/Ar plasma.

representative samples. Because contact angle measurements reflect multiple characteristics of the probed surface, a general consideration of the effects of surface chemistry on contact angle measurements is necessary to interpret these results.

All hydrocarbon polymers have relatively low surface energies. Perfluorinated polymers, such as poly(tetrafluoroethylene) (PTFE), have surface energy values even lower than hydrocarbon polymers. However, with fluorinating plasma treatments of polyolefins, the wetting behavior of the treated polyolefins is complex. Not all types of fluorine-containing functional groups generated during polyolefin fluorination exhibit surface energies that are less than the hydrocarbon groups of PP. Table 1, compiled from a number of sources, lists the estimated surface energy values of several partially fluorinated polymers. Table 1 also identifies the "polar" or "non-dispersive" component of the surface energy for each polymer group.[1,23,24]

The data in Table 1 indicate that perfluorinated CF_2 and CF_3 groups have lower surface energies than CH_2 and CH_3 groups, but CFH groups have higher surface energy and more polar character than these hydrocarbon groups. Comparing the surface energies of PE and poly(vinyl fluoride) reported in Table 1, it is seen that the addition of a single F atom to the PE molecule results in a higher surface energy. However, the entirety of this change in the surface energy is the result of a change in the polar component. This means that the change in surface energy from CF functional groups will be more strongly indicated by polar probe liquids such as water.

Virtually all polymers exhibit contact angle hysteresis, a measured difference between the advancing and receding contact angles, which can be caused by chemical heterogeneity or surface roughness.[25,26] On chemically heterogeneous polymer surfaces, the advancing contact angle is more sensitive to the low-surface-energy components of the surface while the receding angle is more sensitive to the high-energy chemical groups. The advancing angle reaches a maximum at high fractional coverage of the lower-energy component of the heterogeneous surface. Similarly, the receding angle reaches a minimum at high fractional coverage of the high-energy component of a heterogeneous surface.[24,25] This concept is important for interpreting the wettability results for surface-fluorinated PP.

Changes in PP surface topography caused by the fluorination process could potentially complicate the interpretation of contact-angle measurements on plasma-fluorinated surfaces. The advancing and receding contact angles can respond differently to increasing surface roughness. As noted by Wu,[24] a homogeneous surface will show increases in the equilibrium contact angle with increasing roughness if the initial angle is greater than 90° and a decreases in equilibrium contact angle with increasing roughness if the initial angle is less than 90°. However, as explained by Garbassi et al.,[26] for surfaces that exhibit contact angle hysteresis, the advancing contact angle increases as roughness increases while the receding contact angle decreases as roughness increases, regardless of whether the equilibrium contact angle is greater or less than 90°. The roughness effect on advancing and receding contact angles can be more complicated at high degrees of roughness.

The trend of contact-angle response in the reported samples is not correlated to the change in topography observed in the AFM analysis. As previously noted, AFM images of surfaces treated in an F_2 plasma indicate that there is no topographical change in the treated samples during the first stages of fluorination (surfaces with F/C ratios of approximately 0.9 or less). At F/C ratios greater than 0.9, all surfaces show topographical features that

© 2010 WILEY-VCH Verlag GmbH & Co. KGaA, Weinheim
DOI: 10.1002/ppap.200900111

Table 1. Estimated surface energy of various fluorine-substituted polymers.

Polymer	Functional group	Estimated surface energy	
		$mJ \cdot m^{-2}$	
		Total	"Polar" component
Polyethylene	$-CH_2-$	33	0
Polypropylene	$-CH(CH_3)-CH_2-$	30	0
Poly(vinyl fluoride)	$-CH_2-CHF-$	37	6
Poly(vinylidene fluoride)	$-CH_2-CF_2-$	30	7
Polytrifluoroethylene	$-CHF-CF_2-$	24	4
Polytetrafluoroethylene	$-CF_2-CF_2-$	19	0
SAM coatings[a)]	$-CF_2H$ close-packed surface groups	15	?
Polyhexafluropropylene	$-CF(CF_3)-CF_2-$	13	0

[a)]SAM = self-assembled monolayer.

differ from the untreated film surface. This distinction in the AFM observations is contrasted to the observed changes in the contact angles, where the most significant changes in the contact angles occur on surfaces with F/C ratios less than 0.9. Surfaces with F/C ratios greater than 0.9 have much smaller contact angle changes as the degree of fluorination further increases. While surface roughness may affect the contact angle measurements in samples with F/C ratios greater than 0.9, it is reasonably concluded that the observed contact angle response in samples with F/C ratios less than 0.9 are exclusively because of changes in surface chemistry.

The water contact angle values in Figure 10 show a decrease as fluorination is first initiated. ESCA shows that CF groups are the first to develop on the fluorinated PP surface and CF groups are the only possible fluorinated functional group that can produce contact angles lower than the untreated PP. This effect of CF groups would only be seen where there is a minimal presence of CF_2 and CF_3 groups. However, the decrease in water contact angles also occurs in samples that have a non-trivial surface concentration of oxygen, which will also result in decreased water contact angles. In addition, a decreased advancing water contact angle is consistent with a decrease in the concentration of CH_3 groups on the PP surface, possibly indicating an early conversion of CH_3 groups to CH_2F groups or the incorporation of a $CH_2\bullet$ radical into a polymer cross-link. The drop in water contact angles in the early stages of fluorination could be an effect of all three of these surface changes.

After the initial decrease in water contact angles in the early stages of surface fluorination, there is a steady increase in all contact angles as the degree of fluorination increases. This response is consistent with increasing concentrations of CF_2 and CF_3 groups and decreasing or stable concentrations of CF groups. In accordance with the discussion above, relatively small concentrations of CF_2 and CF_3 groups will first affect the advancing contact angles, then a predominant presence of CF_2 and CF_3 groups will raise both the advancing and receding contact angles of all types of liquids relative to the angles measured on unmodified PP. This expected behavior is substantiated by the experimental advancing contact angle data compiled by Wu[24] for water and methylene iodide (diiodomethane, a non-polar liquid).

Between an F/C ratio of 0.9 and the end-state F/C ratio of approximately 1.6, the water contact angles gradually increase, with increasing scatter in the data. Over this same range, the advancing hexadecane angles (and eventually the receding hexadecane angles) appear to reach a plateau, also with increasing scatter in the data. The increasing or stable contact angle measurements, which are more surface sensitive compared with ESCA, are consistent with the increasing CF_2 and CF_3 concentrations observed by ESCA. Stable contact angle values with increasing fluorination as indicated by ESCA are also consistent with a system were the very surface of the treated polymer reaches a highly fluorinated end-state, while the bulk polymer film within the ESCA sampling depth continues to become more fluorinated.

SIMS Results

Because a typical SIMS spectrum from one of the treated PP samples indicates hundreds of different ions, a smaller subset of significant ion clusters, described in Table 2, was examined to facilitate analysis of the SIMS results.

© 2010 WILEY-VCH Verlag GmbH & Co. KGaA, Weinheim

Table 2. Ion clusters identified for ToF-SIMS analysis. High-abundance ions that may be subject to detector saturation, such as CF^+ and CF_3^+, have not been included in these groupings.

H-containing ions (positive ions)	CH_3^+, $C_2H_3^+$, $C_2H_5^+$, $C_3H_5^+$, $C_3H_7^+$, $C_4H_7^+$, $C_4H_9^+$, $C_6H_{11}^+$, $C_8H_{13}^+$, $C_9H_{15}^+$, CFH^+, CFH_2^+, CF_2H^+, $C_3F_4H^+$
Fluorocarbon ions (positive ions)	CF_2^+, $C_2F_5^+$, $C_3F_3^+$, $C_3F_4^+$, $C_3F_5^+$, $C_3F_7^+$, $C_4F_4^+$, $C_4F_7^+$, $C_5F_7^+$, $C_6F_7^+$, $C_5F_9^+$, $C_6F_9^+$, $C_6F_{11}^+$, $C_7F_7^+$, $C_{13}F_{19}^+$, $C_{11}F_{21}^+$, $C_{12}F_{21}^+$, $C_{13}F_{21}^+$, $C_{14}F_{21}^+$, $C_{12}F_{23}^+$, $C_{13}F_{23}^+$, $C_{14}F_{23}^+$, $C_{21}F_{37}^+$
Fluorine-deficient ions (negative ions)	$C_5F_3^-$, $C_6F_3^-$, $C_7F_3^-$, $C_5F_5^-$, $C_6F_5^-$, $C_7F_5^-$, $C_7F_7^-$, $C_9F_9^-$, $C_{10}F_9^-$, $C_{11}F_{11}^-$
Fluorine-rich ions (negative ions)	$C_2F_5^-$, $C_3F_5^-$, $C_3F_7^-$, $C_4F_5^-$, $C_4F_7^-$, $C_5F_7^-$, $C_6F_7^-$, $C_4F_9^-$, $C_5F_9^-$, $C_6F_9^-$, $C_7F_9^-$, $C_8F_9^-$, $C_5F_{11}^-$, $C_6F_{11}^-$, $C_7F_{11}^-$, $C_8F_{11}^-$, $C_9F_{11}^-$, $C_{10}F_{11}^-$, $C_7F_{13}^-$, $C_8F_{13}^-$, $C_9F_{13}^-$, $C_{10}F_{13}^-$, $C_{11}F_{13}^-$, $C_8F_{15}^-$, $C_{12}F_{13}^-$, $C_9F_{15}^-$

Four distinct ion clusters were identified for this analysis:

(i) "Hydrogen-containing" positive ions; species having a composition $C_xF_yH_z^+$, where x and z are positive integers and y is either zero or a positive integer.
(ii) "Fluorocarbon" positive ions; species having a composition $C_xF_y^+$, where x and y are positive integers.
(iii) "Fluorine-deficient" negative ions; species having a composition $C_xF_y^-$, where $y \leq x$, and x and y are positive integers.
(iv) "Fluorine-rich" negative ions; species having composition $C_xF_y^-$, where $y > x$, and x and y are positive integers.

The ratio of hydrogen-containing positive ions to fluorocarbon positive ions, as a function of the ESCA F/C ratio, is shown in Figure 12. Also included on this Figure is an identical analysis of a PTFE polymer reference standard. This plot demonstrates that, as fluorine atoms are added to the polymer, they replace hydrogen atoms, causing a decrease in the number of hydrogen-containing ions that can be formed in the ToF-SIMS analysis. As the degree of fluorination increases, the concentration of all H-containing ions approaches levels seen in PTFE. The fact that the PTFE ESCA F/C ratio of 2.0 is not achieved in the fluorinated PP samples despite the extremely small number of H-containing ions suggests the development of a cross-linked polymer, which would allow fewer sites for fluorine attachment.

The ratio of fluorine-deficient negative ions to fluorine-rich negative ions as a function of the ESCA F/C ratio is shown in Figure 13. As the F/C ratio increases above 0.4, the amount of fluorine-deficient ions falls off dramatically in comparison with the amount of fluorine-rich ions. Similar to the ratio plotted in Figure 12, the F-deficient/F-rich ratio at high fluorination levels approaches, but does not quite reach, that observed for PTFE. This difference between the reported sample with the highest degree of fluorination and

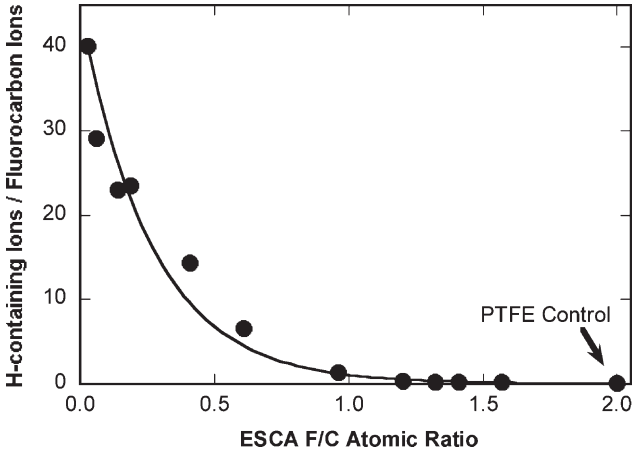

Figure 12. Ratio of ToF-SIMS hydrogen-containing positive ions to fluorocarbon positive ions as a function of ESCA F/C ratio for PP exposed to an F_2/Ar plasma. A PTFE reference is also shown.

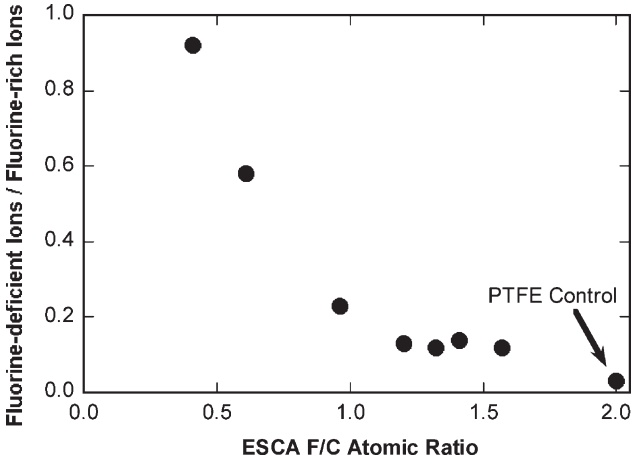

Figure 13. Ratio of ToF-SIMS fluorine-deficient negative ions to fluorine-rich negative ions as a function of ESCA F/C ratio for PP exposed to an F_2/Ar plasma. The ToF-SIMS ratio is not plotted below an F/C ratio of 0.4 due to an absence of negative fluorocarbon ion signal below this value. A PTFE reference is also shown.

© 2010 WILEY-VCH Verlag GmbH & Co. KGaA, Weinheim
DOI: 10.1002/ppap.200900111

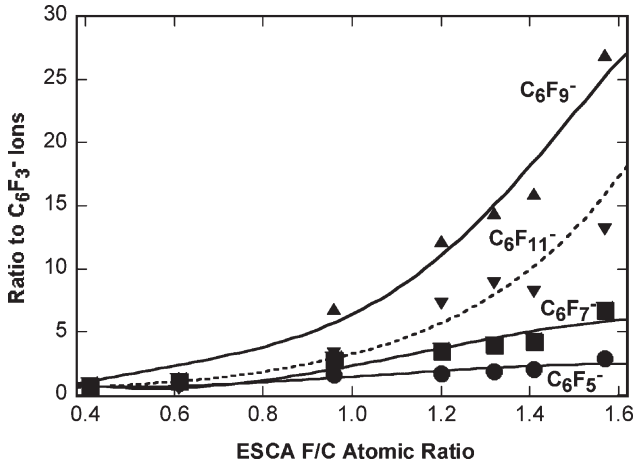

Figure 14. Ratio of ToF-SIMS $C_6F_5^-$, $C_6F_7^-$, $C_6F_9^-$, and $C_6F_{11}^-$ ion counts to the $C_6F_3^-$ ion count, as a function of ESCA F/C ratio, for PP exposed to an F_2/Ar plasma.

PTFE indicates that the reported sample is less linear or more cross-linked than PTFE.

In Figure 13, The F-deficient/F-rich ratio is not plotted below an F/C ratio of 0.4 due to an absence of negative fluorocarbon ion signal below this value. This response suggests that the point where F/C is equal to 0.4 is where adjacent carbon atoms start to become fluorinated. When the F/C ratio is less than 0.4, the modified polymer may predominantly consist of fluorinated carbon atoms located between hydrogenated carbon atoms.

The change in abundance in one series of ions ($C_6F_5^-$, $C_6F_7^-$, $C_6F_9^-$, and $C_6F_{11}^-$) relative to the fluorine-deficient $C_6F_3^-$ ion is shown in Figure 14. The more-fluorinated $C_6F_n^-$ ions increase in relative abundance as the F/C ratio increases. However, the ion with the greatest increase in abundance in this series is $C_6F_9^-$, not the most fluorine-rich ion, $C_6F_{11}^-$. For PTFE, which is not shown in Figure 14, the $C_6F_{11}^-$ ion is more abundant than the $C_6F_9^-$ ion. Ion ratios similar to PTFE should eventually be attained for samples of randomly fluorinated PP because, on a purely statistical basis, the more fluorine atoms that are in close proximity to carbon atoms, the more fluorine-rich the ToF-SIMS ions should be on average. The observation that a C_6 ion with less fluorination becomes more abundant than a C_6 ion with more fluorination is consistent with the polymer becoming less linear and more cross-linked as the overall degree of fluorination increases.

General Mechanism Issues

Capacitively coupled plasmas such as those used in this work can contain ions, electrons, neutral species, free radicals, and UV radiation. In their studies of F_2-containing plasmas, Corbin et al.[10] concluded that vacuum-UV radiation significantly enhanced the fluorination of polyolefins by forming additional polymer alkyl radicals. However, the experimental system described by Corbin et al. had significant differences compared with our system. Their treatments typically had long exposure times (≈60 min) and a power density more than an order of magnitude higher than the work reported here. Since the effects of VUV exposure accumulate over time, as described in Part 2 of this paper,[11] we would expect that the photolytic effects observed by Corbin et al. are more important to their results.

Corbin et al. also found that the use of a Faraday shield, which reduces the capacitive coupling and accordingly reduces the energy of ions incident onto the film, eliminated observed etching of the surface. When energetic ions impinged on the polymer surface, the fluorinated materials decreased in weight as a function of treatment time, while without ion impingement the substrates increased in weight during fluorination. Anand et al.[7,8] attributed the etching and weight loss to C—C bond breakage from energetic ion bombardment. In the absence of ion bombardment, they identified no chain scission. As with the previously described work of Corbin et al. from the same research group, these treatments were typically done with a significantly higher power density with samples that were mounted directly on an electrode. Ions incident onto the film were therefore more energetic, having been accelerated in the sheath, than a film electrically floating in the plasma. Accordingly, there is reason to believe that Anand's ion effect was amplified in comparison with the system reported here.

In the reaction of a hydrocarbon polymer in an F_2 plasma, there is no deposition of a plasma-polymerized thin film. Deposition of a fluorine-containing plasma polymer is favored by a low gas-phase ratio of CF_n radicals to F atoms in the plasma.[27] In an F_2 plasma, the $[CF_n]/[F]$ ratio is vanishingly small so that the deposition of a plasma polymer is unlikely.

In the fluorination of polymers by non-polymerizing gases such as CF_4, NF_3, or F_2, the primary initiation step for saturated polymers such as PP is hydrogen abstraction by F atoms to form HF.[28] HF is a stable molecule that can easily diffuse away from the reaction site before subsequent reactions with the polymer radical can occur. Hydrogen abstraction by F is also fast and efficient. An informative comparison of the rates of hydrogen abstraction from *n*-butane for various active species is given in Table 3.[29–32] A more detailed analysis of hydrogen abstraction is included in Part 2 of this paper.[11]

Hydrogen abstraction is generally considered to be the rate-limiting step in all surface-modification reactions with polyolefins.[33] Examining the direct fluorination of polyolefins with F_2 gas, Poutsma[34] states, "...whatever

© 2010 WILEY-VCH Verlag GmbH & Co. KGaA, Weinheim

thermochemical barriers to halogenation exist are normally associated with the [hydrogen] abstraction rather than the subsequent atom-transfer step.''

In contrast to $O(^3P)$ atom reactions that occur in oxygen-containing discharges, F-atom reactions do not greatly discriminate between different types of C–H bonds for hydrogen abstraction.[34–37] All carbon atoms on a PP surface are likely to be attacked by F atoms to a similar extent, yielding a random mix of polymer alkyl radicals (R•)

$$RH + F\bullet \rightarrow R\bullet + HF \quad (1)$$

Hydrogen abstraction by F_2 molecules also occurs and, although it is relatively slow (see Table 3), it can still initiate the fluorination reaction:

$$RH + F_2 \rightarrow R\bullet + F\bullet + HF \quad (2)$$

However, the difference in reactivity (many orders of magnitude) at ambient temperatures between F• and F_2 in H-abstraction means that F• is the dominant reactant and that the rate of the fluorination process is dependant almost exclusively on the concentration of F•.

Three types of PP polymer radicals can be formed by a single hydrogen abstraction:

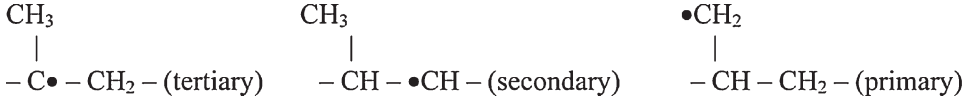

Once polymer radicals are formed, further reactions with gas-phase species, such as F atoms or F_2, are likely to be fast, non-rate-determining reactions.[35–40] The reactions of alkyl radicals with F• are exceptionally fast, probably approaching the encounter frequency:

$$R\bullet + F\bullet \rightarrow RF \quad (3)$$

The reaction of gas-phase alkyl radicals with F_2 is much slower than reaction with F•, as shown in Table 3 and Part 2 of this paper:[11]

$$R\bullet + F_2 \rightarrow RF + F\bullet \quad (4)$$

In F_2 plasmas, it is reasonably assumed that, in addition to a significant quantity of F atoms, there is F_2 present, either from incomplete disassociation of the input F_2 or from the recombination of F atoms. Similarly, in any concentration of F_2 at atmospheric pressure there is some equilibrium quantity of F atoms from disassociation in F_2 gas. At atmospheric pressure this disassociation is estimated as less than 1% at 298 K and 4.6% at 598 K.[2,34] Lower pressures may reduce the disassociated fraction further. This suggests that the main difference between direct and plasma fluorination is the much greater relative concentration of fluorine atoms in the plasma.

We performed multiple experiments exposing our PP film to the same gas flows used in the reported experimentation, but without activating a plasma. These ''no-plasma'' samples showed similar trends in the development of the fluorinated PP surface, up to a maximum F/C ratio of 0.6. The rate of fluorination in our vacuum-pressure no-plasma experiments was at least three orders of magnitude slower than for plasma fluorination. This result contrasts to the atmospheric-pressure reaction of F_2 with hydrocarbon polymers, which has been developed and studied as an industrial process[41,42] but has historically been considered so rapid and exothermic that it is difficult to control.[2]

Table 3. Pertinent reaction rate constants (in $L \cdot mol^{-1} \cdot s^{-1}$).

For gas-phase hydrogen abstraction from *n*-butane:	
By F	4×10^{10}
By OH	1.6×10^{9}
By O (^3P)	1.3×10^{7}
By H	1.5×10^{5}
By CF_3	2.5×10^{4}
By CF_2	$\approx 10^{1}$
By F_2 (from CH_4)	$\approx 10^{1}$
By O_2	Negligible
$CH_4 + F\bullet \rightarrow \bullet CH_3 + HF$	4×10^{10}
$CH_3F + F\bullet \rightarrow \bullet CH_2F + HF$	$\approx 10^{10}$
$CH_2F_2 + F\bullet \rightarrow \bullet CHF_2 + HF$	$\approx 10^{9}$
$CHF_3 + F\bullet \rightarrow \bullet CF_3 + HF$	$\approx 10^{7}$
$\bullet CH_3 + F_2 \rightarrow CH_3F + F\bullet$	8×10^{8}
$\bullet CH_3 + F\bullet \rightarrow$ Products	6×10^{10}
$\bullet CH_2F + F\bullet \rightarrow$ Products	5×10^{10}
$\bullet CF_3 + F\bullet \rightarrow CF_4$	$\approx 10^{10}$
A ''gas kinetic'' or ''encounter frequency'' rate	$\approx 6 \times 10^{10}$

© 2010 WILEY-VCH Verlag GmbH & Co. KGaA, Weinheim
DOI: 10.1002/ppap.200900111

Rate Changes and Gradient Effects

While analysis of the fluorine plasma treatment of PP suggests a relatively simple system, there are several complex elements of the reaction process. As previously noted, the observed rate of the fluorination varies significantly, occurring quite rapidly at first and then more slowly as the PP surface becomes progressively fluorinated. This observation appears to be the effect of two distinct mechanisms: a decrease in reactivity as the PP becomes fluorinated and a gradient of fluorination into the bulk of the PP polymer that spans the ESCA sampling depth.

The decreasing reactivity of the increasingly fluorinated PP is most clearly seen in the nonlinear response of the change in the sample F/C ratio with respect to sample exposure time, shown in Figure 2. There is significant evidence for such deactivation in work that examines the atmospheric-pressure direct fluorination of hydrocarbon materials. In a study of the elemental fluorination of a partially fluorinated alkane (1-fluorobutane), Fredricks and Tedder[43] found that the α and β carbon atoms are deactivated. Fredricks and Tedder state "...in fluorination, further substitution [additional fluorination] really does occur preferentially at sites removed from the substituent halogen atom." They attributed this deactivation to the adverse "polar" effect of the substituent fluorine on the $-CHF-$ group, which should lead to an increase in the activation energy of any subsequent hydrogen-abstraction reaction. Others[2] have suggested that substituent fluorine atoms reduce subsequent hydrogen abstraction because of steric hindrance. Corbin et al.[10] suggest that, as the fluorination of carbon atoms in the starting polymer progresses from CF groups to CF_2 and CF_3 groups, the deactivating effect of substituent fluorine increases, thereby slowing the reaction rate. Corbin et al.[9] state that the "...perfluorination of any polymer with elemental fluorine will necessarily be slow due to the strong deactivation effect of substituent fluorine." Similar results have been seen in low-pressure-plasma fluorination. Yagi and Pavlath[44] found that the treatment of PE with 0.5–1.0 Torr NF_3 plasmas yielded almost exclusively CF and CF_2 functional groups, while the treatment of PP with an NF_3 plasma generated predominantly CF and CF_2 functionalities with only some CF_3.

If the treated PP generally retained the starting molecular structure and hydrogen atoms were randomly replaced with fluorine atoms, then ESCA would always indicate a greater concentration of CF, as compared with CF_2 and CF_3, because this signal will also include CFH and CFH_2 groups that become further fluorinated as the reaction progresses. In addition, as larger groups require more reaction steps to achieve complete fluorinations, CH_3 groups would require the longest time to achieve complete fluorination and CH groups would fluorinate most rapidly. Accordingly, in a random fluorination of an ideal PP surface, the concentration of carbon–fluorine groups indicated by ESCA analysis would always be $CF > CF_2 > CF_3$, until the point of complete fluorination. The deactivation of a surface as it became progressively fluorinated would exacerbate this effect. Our reported results indicate a reaction distinct from the random, homogeneous fluorination of PP. As the observed fluorination progresses to an F/C ratio of 1.0, the indicated CF_2 concentration is higher than CF.

In addition to the overall deactivation effect of the fluorination process, the high relative concentration of CF_2 on the partially fluorinated PP surface also indicates that the progression of the multi-step process required to fully fluorinate the PP on the very surface occurs faster than the progression of the fluorination process into the bulk of the polymer film. The relatively low level of CF can be explained by the outer "layers" of the PP surface (within the ESCA sampling depth) becoming fully fluorinated more quickly than "layers" that are further into the bulk of the PP sample, but still within the ESCA sampling depth. In their F_2 plasma studies, Anand et al.[7,8] estimated that the depth of fluorination was ca. 6 nm in the absence of ion-induced etching.

The contact angle and ToF-SIMS analyses provide additional indications of a gradient of treatment within the ESCA sampling depth. Both contact angles and ToF-SIMS have sampling depths approximately one order of magnitude less than ESCA. As the degree of fluorination detected by ESCA increases above an F/C ratio of 1.2, the contact angle and ToF-SIMS responses stay relatively constant. This comparison suggests that the change in PP chemistry affecting the more surface-sensitive measures reaches completion while the fluorination reaction continues to progress deeper within the ESCA sampling depth.

Change to the PP Molecular Structure

Our analysis suggests that while the average composition of the outermost layers does not change in the final stages of the fluorination reaction, these final steps are accompanied by changes in the polymer structure. In particular, while the contact-angle and ToF-SIMS analyses indicate a relatively unchanging surface above an F/C ratio of 1.2, our analysis indicates significant changes in both the molecular structure and surface topography of samples with progressively higher degrees of fluorination.

Fluorine atoms reacting with the polymer surface cannot directly develop a cross-linked structure in the modified polymer, so cross-links must develop through the reaction of carbon radicals generated on the polymer. However, the polymer fluorination reaction is occurring simultaneously through this same pathway, so that any cross-linking

© 2010 WILEY-VCH Verlag GmbH & Co. KGaA, Weinheim

reactions will necessarily compete with the fluorine-substitution reaction. In the presence of the highly reactive F atoms and F_2, a cross-linking reaction seems unlikely. Iring and Tüdos[45,46] note that at high oxygen concentrations, the oxidation of alkyl radicals in PP is much faster than any other potential cross-linking propagation steps. A cross-linking reaction can only occur in the absence of oxygen.[45–47]

In addition, unlike surface oxidation, fluorination does not directly lead to the scission of the PP backbone and the formation of low-molecular-weight materials. Egitto et al.[48] state, "...for saturated moieties, formation of a radical site on the polymer backbone by hydrogen abstraction does not appear to weaken the polymer structure." Cain et al.[49] have carried out extensive molecular orbital theory calculations on hydrogen abstraction followed by oxygen or fluorine addition. They conclude that "...incorporation of atomic oxygen into the polymer weakens bonds between adjacent carbons. Incorporation of fluorine, on the other hand, has little if any effect on those bonds." Therefore, in low-oxygen-content F_2 plasmas, individual radical-induced hydrogen abstraction events and the subsequent addition of F atoms are unlikely to be accompanied by scission of the PP chain.

Lagow and Margrave[2] suggest that, if individual events in the plasma interaction with the PP film occur nearly simultaneously on adjacent carbon atoms, then there may be a local concentration of energy sufficient to break a main-chain bond. However, this would not necessarily result in the fluorination of the broken bond. When main-chain C–C bonds are broken, the lack of mobility of the polymer chains or "cage" effects in the polymer[38,47,50] causes the radicals formed (–C• and •C–) to remain in close proximity, so that rapid recombination is likely.

Despite these indications that fluorine-radical reactions are unlikely to create polymer cross-links, our results show clear evidence of cross-linking in what appears to be the "end state" of the modified polymer. In the course of our experimentation, we made multiple samples at long exposure times and were not able to produce a sample that showed an ESCA F/C greater than approximately 1.6. In these samples with the highest level of fluorination, ESCA shows a remnant β-shifted CH_n signal that accounts for approximately 10% of the carbon atoms detected. These same samples show negligible hydrogen concentration in the ToF-SIMS analysis. These combined results can only indicate the presence, throughout the ToF-SIMS sampling depth of 1–2 nm, of polymer carbon atoms without either hydrogen or fluorine attached, something which is possible only by new C–C bonds developing in the starting polymer.

In addition, the ToF-SIMS analysis shown in Figure 14 indicates that the polymer becomes more nonlinear as higher degrees of fluorination are reached, particularly above an F/C ratio of 1.0. This indication of a more complex structure becomes evident at approximately the same level of fluorination at which significant change becomes evident in the AFM images. The surface nodules that are seen to develop in the AFM images of the more highly fluorinated samples are consistent with a change to a less-linear structure, which has been shown to develop independently of the chemical change. In comparison, the reported low-fluorination samples show the opposite character of no topography change with significant chemical change.

The ESCA data gives some evidence of what that less-linear structure of the final state might be. In the most fluorinated sample reported here, with an F/C ratio of 1.57, the concentrations of CF, CF_2, and CF_3 are 30%, 45%, and 13%, respectively. If the PP were to be completely fluorinated without change to the molecular structure, each functionality would constitute 33% of the treated surface. This suggests that our highest treatment level has a 3% "deficit" of CF, a 12% "excess" of CF_2, and a 20% "deficit" of CF_3. The end-point deficit of CF_3 and the excess of CF_2, accompanied by the lack of hydrogen, can only result from two effects: the loss of primary carbons from the molecular structure or the incorporation of primary carbons into a polymer cross-link.

The relatively long exposures necessary to create these most highly fluorinated samples allow the accumulation of low-probability effects that we have previously discounted. The ion effects that led to the molecular scission reported by Anand et al.[7] and Hopkins and Badyal[22] potentially accumulate during the development of the PP fluorination process and allow a surface reordering that accompanies the final stages of fluorination in the full ESCA sampling depth.

Part 2 of this paper, a model of the reactions of a fluorine plasma with a PP surface,[11] confirms the importance of accumulated ion effects. The results from this integrated plasma and surface kinetics model show that the effects of ion bombardment and UV illumination are insignificant for the short exposure times that constitute much of our experimental work because the flux of fluorine neutrals to the polymer surface is orders of magnitude greater than the flux of fluorine ions. However, the results also indicate that the minor effects of the ion reactions are irreversible and accumulate with time. At longer exposure times, the cumulative effects of this polymer reordering become evident.

Our plasma modeling work[11] also elucidates one additional factor that occurs early in the reaction process and results in a reordered polymer surface. In the very first steps of reaction with the plasma, the fully hydrogenated PP surface is highly reactive and impinging fluorine atoms are more likely to encounter a hydrogen atom on the surface than a free radical site. These very early steps create a surface rich in radical sites but without the steric hindrance that develops as the surface becomes fluorinated. This creates, in the earliest moments of reaction, a surface with a

© 2010 WILEY-VCH Verlag GmbH & Co. KGaA, Weinheim
DOI: 10.1002/ppap.200900111

greatly increased probability for forming cross-links. This unique reactive state quickly fades, but our model suggests that the cross-linked structure generated in these earliest moments is retained until the endpoint of the reaction.

One potential indication of this early cross-linking is the β-shift CH_n signal evident in the end-state ESCA, indicating the amount of carbon atoms in the end state bound only to other carbons. The size of the β-shift CH_n signal is well correlated with the modeling results[11] and may be related to this early cross-linking. It is reasonably assumed that such structure would be most easily developed through the tertiary carbon and much less likely developed through the primary carbon, because of the large number of non-fluorination reactions involved to develop cross-links involving the primary C atom.

Conclusion

In summary, we used a parallel-plate capacitively coupled vacuum plasma system to investigate the interactions of an F_2-containing plasma with PP film. Our results indicate that the first reactions in this process are fast (significant fluorination in less than 1 s), form some early cross-links, but generally retain the PP structure. The majority of the fluorination process proceeds through hydrogen abstraction and subsequent fluorination of polymer radicals. This fluorination process is accompanied by infrequent, but slowly accumulating, breaks in the polymer backbone and scission of pendant methyl groups from ion exposure. Complete fluorination of the starting polymer is achieved only through reordering of the surface, over much longer periods of time and through a summary effect of low-probability reactions. Particular observed effects include:

(i) ESCA peak shifting and broadening indicate that the fluorination occurs randomly on the PP molecule.
(ii) The evolution of the surface chemistry indicated by ESCA, in addition to the comparison of the ESCA to the more surface-sensitive ToF-SIMS and contact angle analysis results, indicates the deactivation of the fluorinated polymer surface and demonstrates a treatment gradient in the ESCA sampling depth of ca. 10 nm.
(iii) AFM analysis indicates little topographical change until the midpoint of fluorination, then significant change in surface topography between the midpoint and end state of fluorination.
(iv) ToF-SIMS analysis indicates that very small amounts of hydrogen are present on PP films that reached the end state of fluorination. Together with the ESCA, which shows a significant amount of non-fluorinated carbon, this confirms the presence of cross-linking in the end-state samples.
(v) ToF-SIMS shows increasing nonlinearity in the treated PP polymer as the fluorination develops.

In addition, the described experimental results correlate well with Part 2 of this paper in which a model of the F_2 plasma reaction with the PP surface was developed. Together, the experimental work and the reaction model provide a very complete description of this system.

Received: July 9, 2009; Revised: September 25, 2009; Accepted: September 30, 2009; DOI: 10.1002/ppap.200900111

Keywords: cross-linking; fluorination; plasma treatments; polypropylene (PP); surface modification

[1] C.-M. Chan, *Polymer Surface Modification and Characterization*, Hanser-Gardner, Cincinnati 1994, Ch. 2, 3, 6.
[2] R. J. Lagow, J. L. Margrave, "Direct Fluorination: A "New" Approach to Fluorine Chemistry", in: *Progress in Inorganic Chemistry*, Vol. 26, S. J. Leppard, Ed., Wiley-Interscience, New York 1979, p. 161.
[3] M. Strobel, S. Corn, C. S. Lyons, G. A. Korba, *J. Polym. Sci., Part A: Polym. Chem.* **1987**, *25*, 1295.
[4] R. d'Agostino, F. Cramarossa, F. Fracassi, F. Illuzzi, "Plasma Polymerization of Fluorocarbons", in: *Plasma Deposition, Treatment, and Etching of Polymers*, R. d'Agostino, Ed., Academic Press, San Diego 1990, Ch. 2, p. 96.
[5] US 4,264,750 (1981), Massachusetts Institute of Technology, invs.: M. Anand, R. F. Baddour, R. E. Cohen; *Chem. Abstr.* **1981**, *95*, 25915.
[6] US 4,404,256 (1983), Massachusetts Institute of Technology, invs.: M. Anand, R. E. Cohen, R. F. Baddour; *Chem. Abstr.* **1983**, *95*, 25915.
[7] M. Anand, R. E. Cohen, R. F. Baddour, *Polymer* . **1981**, *22*, 361.
[8] M. Anand, R. E. Cohen, R. F. Baddour, "Surface Characterization of Plasma-fluorinated Polymers", in: *Photon, Electron and Ion Probes of Polymer Structure and Properties*, D. W. Dwight, T. J. Fabish, H. R. Thomas, Eds., ACS Symposium Series 162, American Chemical Society, Washington, DC 1981, p. 353.
[9] G. A. Corbin, R. E. Cohen, R. F. Baddour, *Polymer* **1982**, *23*, 1546.
[10] G. A. Corbin, R. E. Cohen, R. F. Baddour, *Macromolecules* **1985**, *18*, 98.
[11] Y. Yang, M. Strobel, S. Kirk, M. J. Kushner, *Plasma Processes Polym.* DOI: 10.1002/ppap.200900114.
[12] D. Briggs, M. J. Hearn, *Vacuum* **1986**, *36*, 1005.
[13] D. Briggs, *Surface Analysis of Polymers by XPS and Static SIMS*, Cambridge University Press, Cambridge 1998, Ch. 2, 4.
[14] W. A. Zisman, *J. Paint Tech.* **1972**, *44*, 42.
[15] E. Occhiello, M. Mora, F. Garbassi, P. Humphrey, J. C. Vickerman, "SSIMS Studies on 18O2 Plasma Treated Polypropylene", in: *Proceedings of the 7th International Conference on SIMS (SIMS7)*, A. Benninghoven, Ed., Wiley, Chichester 1990, p. 789.

© 2010 WILEY-VCH Verlag GmbH & Co. KGaA, Weinheim

[16] G. Beamson, D. Briggs, *High Resolution XPS of Organic Polymers*, Wiley, New York, 1992.
[17] D. T. Clark, W. J. Feast, D. Kilcast, W. K. R. Musgrave, *J. Polym. Sci., Polym. Chem. Ed.* **1973**, *11*, 389.
[18] G. Nansé, E. Papirer, P. Fioux, F. Moguet, A. Tressaud, *Carbon* **1997**, *35*, 175.
[19] A. Tressaud, E. Durand, C. Labrugere, *J. Fluorine Chem.* **2004**, *125*, 1639.
[20] M. Strobel, N. Sullivan, M. C. Branch, V. Jones, J. Park, M. Ulsh, J. M. Strobel, C. S. Lyons, *J. Adhes. Sci. Technol.* **2001**, *15*, 1.
[21] V. Jones, M. Strobel, M. J. Prokosh, *Plasma Processes Polym.* **2005**, *2*, 547.
[22] J. Hopkins, J. P. S. Badyal, *J. Phys. Chem.* **1996**, *100*, 6755.
[23] D. G. Rance, "Thermodynamic Approach to Adhesion Problems", in: *Industrial Adhesion Problems*, D. M. Brewis, D. Briggs, Eds., Wiley-Interscience, New York 1985, Ch. 3.
[24] S. Wu, *Polymer Interface and Adhesion*, Marcel Dekker, New York 1982, Ch. 1, 5.
[25] M. Morra, E. Ochiello, F. Garbassi, *Adv. Colloid Interface Sci.* **1990**, *32*, 79.
[26] F. Garbassi, M. Morra, E. Ochiello, *Polymer Surfaces, From Physics to Technology*, Wiley, Chichester 1994, Ch. 4.
[27] R. d'Agostino, R. Cramarossa, S. De Benedictis, *Plasma Chem. Plasma Process.* **1982**, *1*, 21; *Plasma Chem. Plasma Process.* **1982**, *2*, 213.
[28] J. Hopkins, J. P. S. Badyal, *J. Phys. Chem.* **1995**, *99*, 4261.
[29] R. Atkinson, K. R. Darnall, A. C. Lloyd, A. M. Winer, J. N. Pitts, Jr., *Adv. Photochem.* **1979**, *11*, 375.
[30] J. A. Kerr, S. J. Moss, *CRC Handbook of Bimolecular and Termolecular Gas Reactions*, Volume 1, CRC Press, Boca Raton, Florida 1982.
[31] C. Seeger, G. Rotzoll, A. Lubbert, K. Schugerl, *Int. J. Chem. Kinet.* **1981**, *13*, 39.
[32] National Institute of Standards Chemical Kinetics Database, Standard Reference Database 17, Version 7.0 (Web Version), Release 1.4, http://kinetics.nist.gov/kinetics/index.jsp, **2007**.
[33] M. Strobel, M. C. Branch, M. Ulsh, R. S. Kapaun, S. Kirk, C. S. Lyons, *J. Adhes. Sci. Technol.* **1996**, *10*, 515.
[34] M. L. Poutsma, in: *Free Radicals*, Vol. 2, J. K. Kochi, Ed., Wiley, New York 1973, Ch. 15.
[35] S. J. Moss, A. M. Jolly, B. J. Tighe, *Plasma Chem. Plasma Process.* **1986**, *6*, 401.
[36] I. Tepermeister, H. H. Swain, *J. Vac. Sci. Technol. A* **1992**, *10*, 3149.
[37] J. M. Tedder, in: *Advances in Fluorine Chemistry*, Vol. 2, M. Stacy, J. C. Tatlow, A. G. Sharpe, Eds., Butterworths, London 1961, p. 104.
[38] A. Holländer, J. E. Klemberg-Sapieha, M. R. Wertheimer, *J. Polym. Sci., Part A: Polym. Chem.* **1995**, *33*, **2013**.
[39] C. Decker, A. D. Jenkins, *Macromolecules* **1985**, *18*, 1241.
[40] E. T. Denisov, in: *Mechanisms of Polymer Degradation and Stability*, G. Scott, Ed., Elsevier Applied Science, London 1990, Ch. 1.
[41] A. P. Kharitonov, R. Taege, G. Ferrier, V. V. Teplyakov, D. A. Syrtsova, G.-H. Koops, *J. Fluorine Chem.* **2005**, *126*, 251.
[42] F. J. du Toit, R. D. Sanderson, *J. Fluorine Chem.* **1999**, *98*, 107.
[43] P. S. Fredricks, J. M. Tedder, *J. Chem. Soc.* **1960**, 144.
[44] T. Yagi, A. E. Pavlath, *J. Appl. Polym. Sci. : Appl. Polym. Symp.* **1984**, *38*, 215.
[45] M. Iring, F. Tüdos, *Prog. Polym. Sci.* **1990**, *15*, 217.
[46] M. Iring, F. Tüdos, *Acta Polym.* **1988**, *39*, 19.
[47] J. F. Rabek, *Polymer Photodegradation*, Chapman and Hall, London 1995.
[48] F. D. Egitto, V. Vukanovic, G. N. Tyler, in: *Plasma Deposition, Treatment, and Etching of Polymers*, R. d'Agostino, Ed., Academic Press, San Diego 1990, p. 339.
[49] S. R. Cain, F. D. Egitto, F. Emmi, *J. Vac. Sci. Technol.* **1987**, *A5*, 1578.
[50] D. J. Carlsson, S. Chemla, in: *Mechanisms of Polymer Degradation and Stability*, G. Scott, Ed., Elsevier Applied Science, London 1990, Ch. 4.

© 2010 WILEY-VCH Verlag GmbH & Co. KGaA, Weinheim
DOI: 10.1002/ppap.200900111